A&A 623, A104 (2019)
https://doi.org/10.1051/0004-6361/201834333

Astronomy & Astrophysics

SOPHIE velocimetry of *Kepler* transit candidates

XIX. The transiting temperate giant planet KOI-3680b

G. Hébrard[1,2], A. S. Bonomo[3], R. F. Díaz[4], A. Santerne[5], N. C. Santos[6,7], J.-M. Almenara[8], S. C. C. Barros[6], I. Boisse[5], F. Bouchy[9], G. Bruno[5,10], B. Courcol[5], M. Deleuil[5], O. Demangeon[6], T. Guillot[11], G. Montagnier[1,2], C. Moutou[12], J. Rey[9], and P. A. Wilson[1,13,14]

[1] Institut d'Astrophysique de Paris, UMR7095 CNRS, Université Pierre & Marie Curie, 98bis Boulevard Arago, 75014 Paris, France
e-mail: hebrard@iap.fr
[2] Observatoire de Haute-Provence, CNRS, Université d'Aix-Marseille, 04870 Saint-Michel-l'Observatoire, France
[3] INAF, Osservatorio Astrofisico di Torino, Via Osservatorio 20, 10025, Pino Torinese, Italy
[4] CONICET, Instituto de Astronomía y Física del Espacio (IAFE), Universidad de Buenos Aires, Buenos Aires, Argentina
[5] CNRS, CNES, Laboratoire d'Astrophysique de Marseille, Aix Marseille Université, 13388 Marseille, France
[6] Instituto de Astrofísica e Ciências do Espaço, Universidade do Porto, CAUP, Rua das Estrelas, 4150-762 Porto, Portugal
[7] Departamento de Física e Astronomia, Faculdade de Ciências, Universidade do Porto, Rua Campo Alegre, 4169-007 Porto, Portugal
[8] Université Grenoble Alpes, CNRS, IPAG, 38000 Grenoble, France
[9] Observatoire de Genève, Université de Genève, 51 Chemin des Maillettes, 1290 Sauverny, Switzerland
[10] INAF, Osservatorio Astrofisico di Catania, Via S. Sofia, 78, 95123 Catania, Italy
[11] Université Côte d'Azur, OCA, Lagrange CNRS, 06304 Nice, France
[12] Canada France Hawaii Telescope Corporation, Kamuela, HI 96743, USA
[13] Department of Physics, University of Warwick, Gibbet Hill Road, Coventry, CV4 7AL, UK
[14] Centre for Exoplanets and Habitability, University of Warwick, Gibbet Hill Road, Coventry CV4 7AL, UK

Received 27 September 2018 / Accepted 19 November 2018

ABSTRACT

Whereas thousands of transiting giant exoplanets are known today, only a few are well characterized with long orbital periods. Here we present KOI-3680b, a new planet in this category. First identified by the *Kepler* team as a promising candidate from the photometry of the *Kepler* spacecraft, we establish here its planetary nature from the radial velocity follow-up secured over 2 yr with the SOPHIE spectrograph at Observatoire de Haute-Provence, France. The combined analysis of the whole dataset allows us to fully characterize this new planetary system. KOI-3680b has an orbital period of 141.2417 ± 0.0001 days, a mass of 1.93 ± 0.20 $M_{\rm Jup}$, and a radius of 0.99 ± 0.07 $R_{\rm Jup}$. It exhibits a highly eccentric orbit (e = 0.50 ± 0.03) around an early G dwarf. KOI-3680b is the transiting giant planet with the longest period characterized so far around a single star; it offers opportunities to extend studies which were mainly devoted to exoplanets close to their host stars, and to compare both exoplanet populations.

Key words. planetary systems – techniques: radial velocities – techniques: photometric – techniques: spectroscopic – stars: individual: KOI-3680

1. Introduction

By continuously monitoring the light curves of 156 000 stars from May 2009 to May 2013 with high photometric accuracy, the *Kepler* spacecraft revealed more than 4500 transiting planet candidates. These *Kepler* objects of interest (KOIs) have corresponding radii ranging from giant planets even larger than Jupiter down to Earth-like planets smaller than our Earth. They also cover a wide span of distances from their host stars, with orbital periods of several hours, days, or months.

Whereas several purely stellar configurations can mimic planetary transits, in particular those involving blended binaries, three main methods have been used to distinguish genuine planets from false positives in the KOI sample. First, from Bayesian statistics of the *Kepler* light curves and comparison of astrophysical configuration probabilities, it is possible to validate the planetary nature of a transit. About half of the KOIs were validated this way, including more than 800 transiting planets in multiple systems by Rowe et al. (2014; see also Lissauer et al. 2012, 2014) and nearly 1300 additional planets by Morton et al. (2016). That validation technique however does not allow the mass of the planets to be measured, which is a particularly important parameter for their characterization and study.

The second technique relies on measurements of transit timing variations (TTVs) in multi-planet systems and is also mainly based on the *Kepler* light curves (e.g. Holman et al. 2010; Fabrycky et al. 2012; Ford et al. 2012). Tens of KOIs were identified as planets and their masses measured using such dynamic analyses of mutual gravitational interactions.

The third method requires additional ground-based high-resolution spectroscopic observations. These allow the planetary nature of a KOI to be established or rejected, as well as the mass of the identified planets to be measured thanks to the induced stellar radial velocity (RV) variations. This is the historical method to characterize transiting planet candidates from ground- and space-based photometric surveys, and was used to

characterize tens of KOIs (e.g. Bonomo et al. 2014; Hébrard et al. 2014; Marcy et al. 2014; Buchhave et al. 2016). Today, the transit light curve in addition to TTV and RV analyses provides the most comprehensive way of obtaining exoplanetary properties, that is, measured orbital and physical parameters of planets, including period, eccentricity, mass, and radius.

An RV follow-up of KOIs was begun in 2010 with the SOPHIE spectrograph at the 193-cm Telescope of the Observatoire de Haute-Provence, France. The program allowed us to announce and characterize new transiting companions, including hot Jupiters (e.g. Santerne et al. 2011; Bonomo et al. 2012a; Deleuil et al. 2014; Almenara et al. 2015), brown dwarfs (e.g. Díaz et al. 2013; Moutou et al. 2013), and low-mass stars (e.g. Ehrenreich et al. 2011; Bouchy et al. 2011; Díaz et al. 2014), as well as to put constraints on systems presenting TTVs (Bruno et al. 2015; Almenara et al. 2018). The occurrence rate and physical properties of giant planets with up to 400-day orbital periods were moreover constrained from this program, which also revealed a high false-positive rate among the corresponding KOIs (Santerne et al. 2012, 2016).

The same program also allowed us to announce and characterize the new transiting giant planet KOI-1257b on a particularly long orbital period of 86.6 days (Santerne et al. 2014). Only a few transiting planets are well characterized with periods of a few tens of days or longer. Indeed, the geometric probability for the orbital plane to be aligned with the line of sight roughly scales with the power −5/3 of the orbital period (Beatty & Gaudi 2008). For orbital periods around 100 days, the geometric transit probability is on the order of 1%, and when the alignment is good enough to produce transits, opportunities to observe them are rare due to the long period. Thus, in addition to KOI-1257b, only a few transiting, long-period planets are well characterized today; examples include HD 80606b (Moutou et al. 2009; Hébrard et al. 2011), CoRoT-9b (Deeg et al. 2010; Bonomo et al. 2017a), or Kepler-432b (Ciceri et al. 2015) characterized with long-time-span RVs, and the multiple systems Kepler-30 (Sanchis-Ojeda et al. 2012), Kepler-79 (Rowe et al. 2014), and Kepler-87 (Ofir et al. 2014) characterized with TTVs. Also classified using TTVs are some long-period, transiting planets orbiting binary stars, as in the systems Kepler-16 (Doyle et al. 2011), Kepler-34, and Kepler-35 (Welsh et al. 2012).

The vast majority of well-characterized transiting planets have short orbital periods and receive high irradiation from their host star. They are particularly interesting (e.g. Winn 2010) because their physics as well as their formation and evolution processes can be constrained. Indeed, it is possible to measure the bulk density of transiting planets, permitting studies of their internal structure, as well dynamic analyses through obliquity measurements, or through TTVs in cases of multiple systems. They also allow atmospheric studies in absorption through transits and in emission through occultation for the brightest host stars. Therefore, there is great interest in extending such powerful analyses from close-in planets to less irradiated ones. To do that, new transiting, long-period planets need to be detected and characterized. Long-period, giant planets present additional interest as some of them are the probable precursors of the observed and well-studied population of hot Jupiters. Studying more-temperate planets could also put important constraints on the migration processes and their effects on the internal structure and atmosphere of migrating planets.

Here we present KOI-3680b, a new transiting, long-period planet. The planet candidate was revealed with an orbital period of 141 days by Wang et al. (2013) and Rowe et al. (2015) as KOI-3680.01. Its transit depth was characteristic of a giant planet. Both analyses used the Quarters Q1 to Q12 representing 3 yr of *Kepler* observations. Furthermore, this candidate was not detected in the previous releases of *Kepler* data (Borucki et al. 2011a,b; Batalha et al. 2013), illustrating the need for long time-span data to detect such long-period events. Here, an additional cause was the fact that the first three transits unfortunately fell within gaps in the time series (see Sect. 2.1 and Fig. 1). Morton et al. (2016) computed the false-positive probability of KOI-3680.01 to be 1.20 ± 0.15% so could not reach a definitive conclusion about its nature. Therefore, it remained undetermined whether these transits were caused by a planet or another scenario.

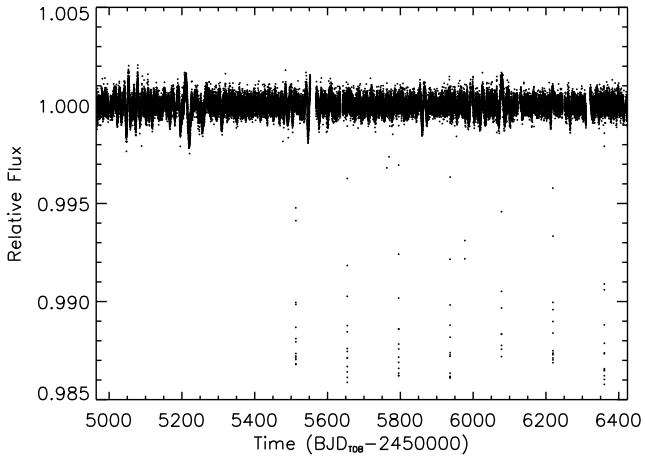

Fig. 1. *Kepler* light curve showing the transits of KOI-3680.01 and a low-amplitude variability due to the rotational modulation of photospheric active regions. The first three transits unluckily fell within gaps in the time series.

Our RV follow-up with SOPHIE allows us to show they are caused by a planet and to characterize the parameters of the planetary system. We describe the photometric and spectroscopic observations of the object in Sect. 2 and the analysis of the whole dataset and the results in Sect. 3. We discuss our results in Sect. 4 and conclude in Sect. 5.

2. Observations and data reduction

2.1. Photometric detection with Kepler

The IDs, coordinates, and magnitudes of the star KOI-3680 are reported in Table 1. *Kepler* photometric data were retrieved from the MAST archive[1]; they were acquired only in long-cadence mode, that is, with a temporal sampling of 29.4 min over 4 yr from 13 May 2009 to 11 May 2013 (quarters Q1 to Q17). We used the *Kepler* light curves as reduced by both the Simple Aperture Photometry (SAP) and Pre-search Data Conditioning (PDC) *Kepler* pipelines (Jenkins et al. 2010). Those data are described in the DR25 *Kepler* catalogue (Thompson et al. 2018).

The PDC light curve, which is shown in Fig. 1, clearly presents seven transits with a depth of about 1.4%. Three more transits should have been observed by *Kepler* at BJD$_{TDB}$ − 2 450 000 < 5500 (see Fig. 1) but, unfortunately, they all fell in data gaps caused by *Kepler* operational activities, such as safe modes and pointing tweaks (Jenkins et al. 2010). Moreover, the fifth transit observed at 6077.8960 BJD$_{TDB}$ −2 450 000 misses the egress and is thus partial. We note that individual transits seem

[1] http://archive.stsci.edu/kepler/data_search/search.php

Table 1. IDs, coordinates, and magnitudes of the planet-host star.

Kepler object of interest	KOI-3680
Kepler exoplanet catalog	Kepler-1657
Kepler ID	9025971
2MASS ID	J19330757+4518348
Gaia ID	2126518783059463168
RA (J2000)	19:33:07.574
Dec (J2000)	+45:18:34.81
Gaia parallax (mas)	1.056 ± 0.027
Distance (pc)	950 ± 25
RA PM (mas yr^{-1})	−11.51 ± 0.04
Dec PM (mas yr^{-1})	−3.60 ± 0.04
Kepler magn. K_p	14.524
Howell Everett Survey Johnson-*B*	15.47
Howell Everett Survey Johnson-*V*	14.77
Gaia-*G*	14.50269 ± 0.00026
Gaia-BP	14.880 ± 0.002
Gaia-RP	13.974 ± 0.001
2MASS-*J*	13.384 ± 0.021
2MASS-*H*	13.041 ± 0.027
2MASS-K_s	13.101 ± 0.039

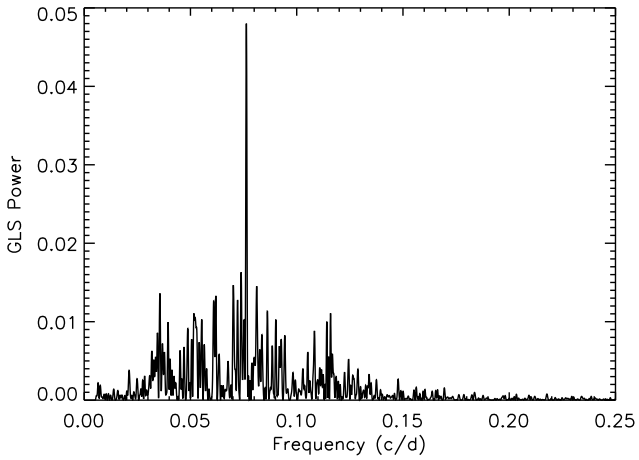

Fig. 2. Generalized Lomb–Scargle periodogram of the *Kepler* light curve. The highest peak at ν = 0.0763 c/d, which corresponds to a period of 13.10 days, is likely related to the stellar rotation period.

to vary in depth in Fig. 1. This is mainly due to transits occurring during small bumps or ditches in the light curve due to stellar activity not yet corrected at that stage. To a less extent this could also be due to possible residual background as well as possible instrumental effects. In the analysis presented below in Sect. 3.2, the phase-folded curve is normalized around each transit to correct for stellar activity. The final uncertainty on the planetary radius accounts for possible residual, though not significant, differences in the depth of individual transits.

After removing the transits of KOI-3680.01, we searched for additional transit signals due to possible coplanar planetary companions using a modified version of the pipeline described by Bonomo et al. (2012b) but found none; there is thus no evidence for a multiple transit system.

The *Kepler* light curve also shows low-amplitude variability with a maximum peak-to-peak variation of ~0.4% (Fig. 1), which is likely due to the rotational modulation of photospheric starspots and/or faculae. Despite the low amplitude, the

Table 2. SOPHIE measurements of the planet-host star KOI-3680.

BJD$_{UTC}$ −2 450 000	RV (km s^{-1})	±1 σ (km s^{-1})	Bisect.^{a} (km s^{-1})	Exp. (s)	S/N^b
6900.5292	−44.880	0.017	−0.069	3600	16.2
6935.3558	−45.082	0.024	0.002	3600	16.3
6948.3726	−45.020	0.012	−0.044	3600	23.2
6975.3101	−44.923	0.016	−0.018	3600	20.0
6982.3470	−44.919	0.016	−0.054	3600	21.9
7107.6489	−44.878	0.026	0.002	3164	18.2
7192.5683	−44.912	0.020	0.005	3600	16.7
7211.4976	−44.922	0.034	−0.027	3600	11.9
7219.4596	−45.063	0.030	−0.088	2452	12.4
7225.4649	−45.016	0.015	−0.017	3600	19.8
7241.4781	−44.951	0.019	−0.027	3600	18.1
7246.4579	−44.948	0.022	−0.051	3600	16.1
7261.3529	−44.905	0.017	−0.047	3600	18.3
7265.4376	−44.917	0.019	0.026	3600	18.1
7276.4394	−44.913	0.014	0.024	3600	17.3
7303.3809	−44.871	0.022	0.050	3600	13.5
7334.3829	−44.929	0.025	−0.034	3443	17.4
7346.2494	−44.988	0.038	0.039	2704	10.8
7352.2475	−44.954	0.032	−0.046	3600	14.1
7359.2618	−45.063	0.015	−0.032	3600	19.1
7379.2595	−44.952	0.036	−0.002	2801	15.0
7607.4763	−44.871	0.016	−0.054	3600	15.8
7623.5069	−44.884	0.022	−0.029	3600	16.0
7628.5428	−44.951	0.020	−0.030	3600	14.4
7659.3588	−44.980	0.019	−0.085	3600	14.3

Notes. $^{(a)}$Bisector spans; error bars are twice those of the RVs. $^{(b)}$Signal-to-noise ratio per pixel at 550 nm.

Generalized Lomb–Scargle (GLS) periodogram (Zechmeister & Kürster 2009) of the light curve uncovers a significant periodicity at 13.102 ± 0.002 days (Fig. 2). This periodicity could be related to the stellar rotation period (see below Sect. 3.1). Following the approach of Czesla et al. (2009), we estimate the impact of unocculted starspots on the transit depth to be 24 ppm at most, which is negligible here.

After removing the transits and low-frequency stellar variations, the rms of the light curve is 245 ppm, which is almost equal to the average of the uncertainties of the photometric measurements, that is, 235 ppm. So there are no signs of remaining noise or additional signals.

2.2. Radial-velocity follow-up with SOPHIE

We observed KOI-3680 with the SOPHIE spectrograph, first to establish the planetary nature of the transiting candidate, then to characterize the secured planet by measuring in particular its mass and orbital eccentricity. SOPHIE is dedicated to high-precision RV measurements at the 1.93-m telescope of the Haute-Provence Observatory (Perruchot et al. 2008; Bouchy et al. 2009a, 2013). We used its high-efficiency mode with a resolving power R = 40 000 and slow readout mode to increase the throughput for this faint star. We obtained 28 observations between August 2014 and September 2016 but three of them were not used due to their poor quality. Exposure times were 60 min, except for five observations where it was slightly shorter. The signal-to-noise ratios (S/N) per pixel at 550 nm range between 14 and 25 depending on the exposure and weather conditions (Table 2).

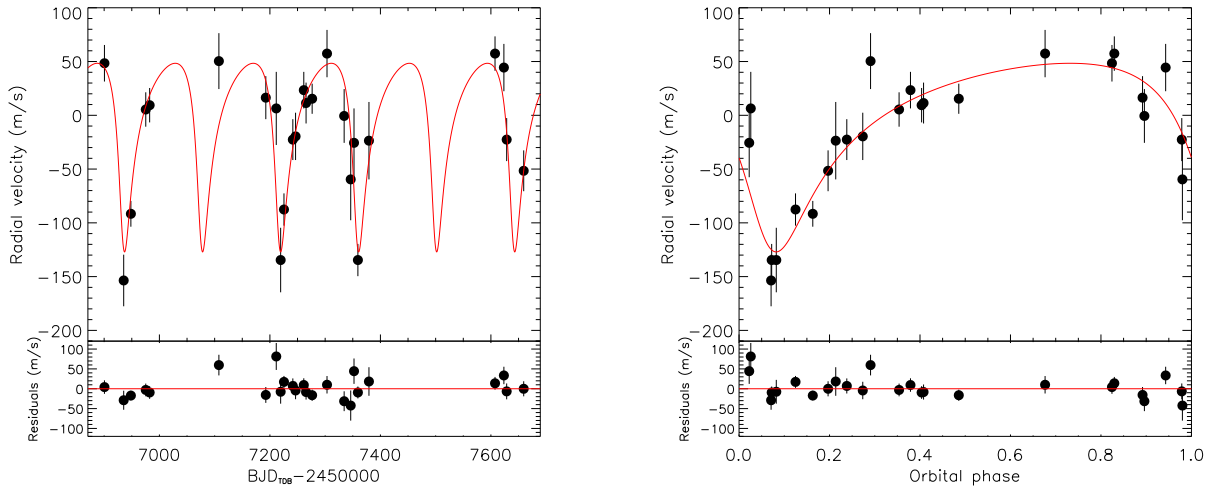

Fig. 3. *Left panel*: SOPHIE radial velocities of KOI-3680 as a function of time and the best Keplerian model (red solid line). *Right panel*: as in the left panel but as a function of the orbital phase (transits occur at phase equal to zero/one). On both plots the lower panel displays the residuals.

The spectra were extracted using the SOPHIE pipeline (Bouchy et al. 2009a) and the radial velocities were measured from the weighted cross-correlation with a numerical mask characteristic of the spectral type of the star (Baranne et al. 1994; Pepe et al. 2002). They were corrected from the CCD charge transfer inefficiency (Bouchy et al. 2009b) and their error bars were computed from the cross-correlation function (CCF) using the method presented by Boisse et al. (2010). Following the procedure adopted by Santerne et al. (2016), we used a G2-type mask and corrected for instrumental drifts in the RV using those measured on the constant star HD 185144 on the same nights. The causes for these instrumental drifts are not well understood or identified but might be due to thermal effects. Their dispersion is 5 m s^{-1} over the nights where KOI-3680 was observed; we corrected for this effect despite its low amplitude because that correction does not add significant extra RV uncertainty.

Nine spectra were polluted by moonlight but the RV of the Moon signal was shifted by at least 32 km s^{-1} from the RV of KOI-3680. Such shifts are large enough to avoid significant perturbation on the stellar RV. Indeed, the median moonlight correction (done thanks to the second SOPHIE aperture located on the sky background 2′ away from the first aperture located on the star; see e.g. Hébrard et al. 2008; Bonomo et al. 2010) here is 15 m s^{-1} which is smaller than the typical accuracy of our RV measurements. As the moonlight correction could add extra uncertainty on the final RV (due to the noise present in the second-aperture spectra), we decided not to correct for this pollution. As an additional test, we checked that the Keplerian solution ignoring these nine Moon-polluted spectra agrees within 1 σ with our final solution using the whole dataset.

The resulting CCFs have full width at half maximum (FWHM) of 9.9 ± 0.1 km s^{-1} and contrast that represents ∼30% of the continuum. The lines are slightly broader than what is usually measured in high-efficiency mode due to the stellar rotation of KOI-3680 (we measure $v \sin i_* = 3.5 \pm 1.0$ km s^{-1} from the CCF width; see Sect. 3.1). The radial velocities have accuracies ranging from ±12 to ±38 m s^{-1} depending on the S/N, with a median value of ±20 m s^{-1}. They are reported in Table 2 and displayed in Fig. 3 together with their Keplerian fits and their residuals. They show significant variations in phase with the *Kepler* transit ephemeris, for an eccentric orbit and a semi-amplitudes of the order of 100 m s^{-1}. This implies a companion mass in the planet regime.

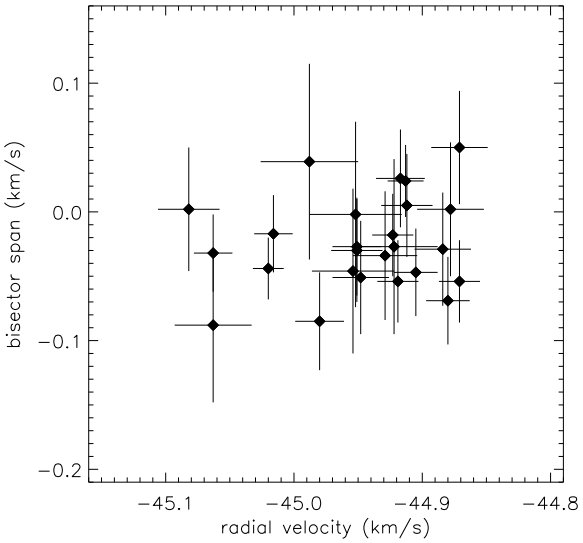

Fig. 4. Bisector span as a function of the radial velocities with 1-σ error bars. The ranges extend equally on the x- and y-axes. The bisector spans show a smaller dispersion than the RVs, and no correlation is seen between the two quantities.

Radial velocities measured using different stellar masks (F0, K0, or K5) produce variations with similar amplitudes (in agreement within 0.8, 0.7, and 1.1 σ, respectively) to those obtained with the G2 mask, so it is unlikely that these variations are produced by blend scenarios composed of stars of different spectral types. Similarly, the measured CCF bisector spans (Table 2) quantify possible shape variations of the spectral lines. They show a dispersion of 36 m s^{-1} which is 1.7 times smaller than the RV dispersion, whereas each bisector span is roughly two times less precise than the corresponding RV measurement. Therefore, the bisector spans show no significant variations. Moreover, they show no correlations with the RVs as shown in Fig. 4. The linear correlation parameter is +0.10 ± 0.12 and the Pearson and Spearman's rank correlation factors have low values of 0.18 and 0.12, respectively. This reinforces the conclusion that the RV variations are not caused by spectral-line profile changes attributable to blends or stellar activity. We therefore conclude that the event KOI-3680.01 is due to a transiting planet, which we designate as KOI-3680b hereafter.

3. System characterization

3.1. Spectral analysis of the host star

Stellar atmospheric parameters ($T_{\rm eff}$, $\log g$, microturbulence $\xi_{\rm t}$ and [Fe/H]) and respective error bars were derived using the methodology described in Sousa et al. (2008) and Santos et al. (2013). In brief, we make use of the equivalent widths of 153 Fe I and 22 Fe II lines, and we assume ionization and excitation equilibrium. The process makes use of a grid of Kurucz model atmospheres (Kurucz 1993) and the radiative transfer code MOOG (Sneden 1973).

The equivalent widths were measured on a SOPHIE spectrum built from the addition of the existing high-resolution spectra used for the RV measurements, but excluding the SOPHIE spectra presenting Moonlight contamination. The resulting average SOPHIE spectrum has a S/N of ∼40 as measured in continuum regions near 6600 A. We obtained $T_{\rm eff} = 5830 \pm 100$ K, $\log g = 4.49 \pm 0.13$ (cgs), $\xi_{\rm t} = 1.20 \pm 0.13\,{\rm km\,s^{-1}}$, and [Fe/H] = 0.16 ± 0.07. Using the calibration of Torres et al. (2010) with a correction following Santos et al. (2013), we derive a mass and radius of $1.04 \pm 0.05\,M_\odot$ and $0.96 \pm 0.16\,R_\odot$, respectively. Those values of $T_{\rm eff}$ and [Fe/H] are used as input in the analysis below (Sect. 3.2). Our derived stellar parameters agree within $1\,\sigma$ with those reported by the *Kepler* mission in the DR25 catalogue (Thompson et al. 2018). DR25 values are $T_{\rm eff} = 5705^{+104}_{-115}$ K, $\log g = 4.397^{+0.095}_{-0.105}$ (cgs), [Fe/H] = 0.00 ± 0.15, $M_* = 0.941^{+0.068}_{-0.056}\,M_\odot$, and $R_* = 1.017^{+0.147}_{-0.107}\,R_\odot$.

We also derived the projected rotational velocity $v \sin i_* = 3.5 \pm 1.0\,{\rm km\,s^{-1}}$ from the parameters of the CCF using the calibration of Boisse et al. (2010). This implies a stellar rotation period upper limit $P_{\rm rot} < 13.9^{+5.5}_{-3.1}$ days, in agreement with the value $P_{\rm rot} \simeq 13.10$ days derived in Sect. 2.1.

Therefore, KOI-3680 is an early G dwarf.

3.2. Parameters of the planetary system

To determine the KOI-3680 system parameters, we simultaneously modelled the *Kepler* photometry and the SOPHIE RVs in a Bayesian framework. We did not include a Rossiter-McLaughlin model because no RVs were obtained during a KOI-3680b transit. We employed a differential evolution Markov chain Monte Carlo (DE-MCMC) technique (Ter Braak 2006; Eastman et al. 2013) using a Keplerian orbit and the transit model of Mandel & Agol (2002). Following Bonomo et al. (2015), we normalized the transits after accounting for the stellar crowding values provided by the *Kepler* team for each quarter, and oversampled the transit model at 1 min to overcome the smearing effect due to the long-cadence integration times on the determination of transit parameters (Kipping 2010). The activity level of the star deduced from the low-amplitude flux variability allows us to assume that possible unocculted starspots and/or faculae do not significantly affect the measurement of the transit depth (Sect. 2.1). Given the relatively large star–planet distance of 0.33 AU at inferior conjunction, we accounted for a light travel time of ∼2.7 min between the *Kepler* transit observations (which refer to the planet reference frame) and the RV observations (which refer to the stellar reference frame).

Our global model has 12 free parameters: the mid-transit time $T_{\rm c}$; the orbital period P; the systemic RV γ; the RV semi-amplitude K; $\sqrt{e}\cos\omega$ and $\sqrt{e}\sin\omega$, where e and ω are the orbital eccentricity and argument of periastron; the RV uncorrelated jitter term $s_{\rm j}$ (e.g., Gregory 2005); the transit duration T_{14}; the scaled planetary radius $R_p/R_\star$; the orbital inclination i_p; and the two limb-darkening coefficients q_1 and q_2, which are related to the coefficients u_1 and u_2 of the quadratic limb-darkening law (Claret 2004; Kipping 2013). We used uninformative priors on all the parameters with bounds of [0, 1[for the eccentricity and [0, 1] for the q_1 and q_2 limb-darkening parameters (Kipping 2013). We ran 24 chains, which is twice the number of free parameters. The step orientations and scales for each chain were automatically determined from two of the other chains that were randomly selected at each step (Ter Braak 2006); a proposal step was accepted or rejected according to the Metropolis–Hastings algorithm, by using a Gaussian likelihood function. We adopted the prescriptions given by Eastman et al. (2013) for the removal of burn-in steps and the convergence check. The best-fit models of the radial velocities and transits are displayed in Figs. 3 and 5. The radial velocities fit well with the photometric period and phase, and show no hints of additional signals. Any additional RV drift, which could be the signature of a long-period companion in the system, should be smaller than $15\,{\rm m\,s^{-1}\,yr^{-1}}$.

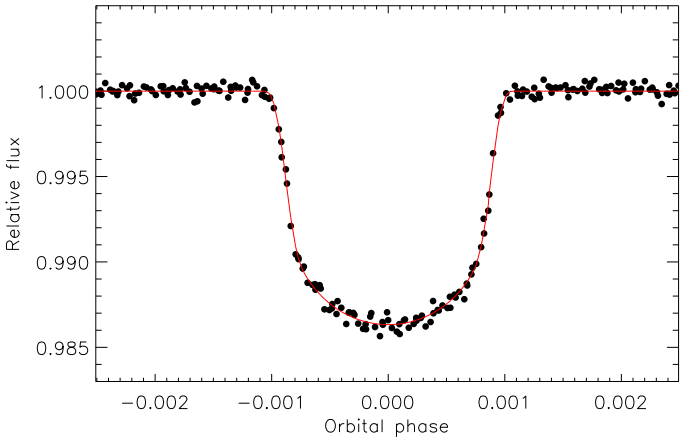

Fig. 5. Phase-folded transit of KOI-3680b along with the best-fit model (red solid line).

The stellar density derived from the transit fitting was used as a proxy for stellar luminosity, along with the stellar metallicity and effective temperature initially derived in Sect. 3.1. They were used to determine the stellar parameters, that is, mass, radius, and age, through the Yonsei-Yale evolutionary tracks (Demarque & Kim 2004; see Bonomo et al. 2014 for further details). Fully consistent stellar parameters were also found with the Dartmouth stellar models (Dotter et al. 2008). The final values and 1σ uncertainties of the stellar, orbital, and planetary parameters were computed as the medians and the [15.87−84.13]% interval of their posterior distributions and are listed in Table 3; more specifically, we considered 34.13% quantiles above the medians and 34.13% quantiles below the medians to allow for possibly asymmetric error bars. The stellar gravity derived here ($\log g = 4.473^{+0.027}_{-0.034}$ cgs) agrees with that obtained from the spectral analysis above ($\log g = 4.49 \pm 0.13$; Sect. 3.1) but is more precise; this shows the good consistency of those studies.

These values also agree with those from the *Gaia* DR2 (Gaia Collaboration 2018). More specifically, our derived stellar radius $R_\star = 0.96^{+0.05}_{-0.06}\,R_\odot$ is compatible within 1σ of that estimated from the *Gaia* data, that is, $R_\star = 1.01 \pm 0.05\,R_\odot$ (Berger et al. 2018). However, we report the latter estimate for comparison and do not consider it necessarily more reliable than our value of $R_\star$, because it was derived from a bolometric correction that in turn relies on stellar models (Berger et al. 2018).

Table 3. KOI-3680 system parameters.

Stellar parameters	
Star mass ($M_\odot$)	$1.01^{+0.07}_{-0.16}$
Star radius ($R_\odot$)	$0.96^{+0.05}_{-0.06}$
Stellar density ρ_* (g cm^{-3})	$1.88^{+0.40}_{-0.34}$
Age t (Gyr)	$3.2^{+9.6}_{-2.3}$
Effective temperature $T_{\rm eff}$(K)	5830 ± 100
Spectroscopic surface gravity log g (cgs)	4.49 ± 0.13
Derived surface gravity log g (cgs)	$4.473^{+0.027}_{-0.034}$
Metallicity [Fe/H] (dex)	0.16 ± 0.07
Projected rotational velocity $v \sin i_*$ (km s^{-1})	3.5 ± 1.0
Kepler limb-darkening coefficient q_1	$0.30^{+0.08}_{-0.07}$
Kepler limb-darkening coefficient q_2	$0.46^{+0.11}_{-0.08}$
Kepler limb-darkening coefficient u_a	0.51 ± 0.05
Kepler limb-darkening coefficient u_b	0.04 ± 0.11
Systemic velocity $V_{\rm r}$ (km s^{-1})	−44.9284 ± 0.0044
Transit and orbital parameters	
Orbital period P (days)	141.241671 ± 0.000086
Transit epoch T_0[BJD$_{\rm TDB}$−2 450 000]^a	5936.65434 ± 0.00018
Transit duration T_{14} (days)	0.2807 ± 0.0012
Radius ratio $R_{\rm p}/R_*$	$0.10646^{+0.00079}_{-0.00059}$
Inclination i_p (deg)	$89.892^{+0.069}_{-0.086}$
a/R_*	125.7 ± 8.4
Impact parameter b	$0.15^{+0.10}_{-0.09}$
$\sqrt{e}\ \cos\omega$	$0.300^{+0.086}_{-0.091}$
$\sqrt{e}\ \sin\omega$	$-0.635^{+0.046}_{-0.037}$
Orbital eccentricity e	0.496 ± 0.031
Argument of periastron ω (deg)	154.7 ± 7.8
Radial-velocity semi-amplitude K (m s^{-1})	87.7 ± 6.6
Planetary parameters	
Planet mass $M_{\rm p}$ ($M_{\rm Jup}$)	$1.93^{+0.19}_{-0.21}$
Planet radius $R_{\rm p}$ ($R_{\rm Jup}$)	$0.99^{+0.06}_{-0.07}$
Planet density $\rho_{\rm p}$ (g cm^{-3})	$2.46^{+0.42}_{-0.36}$
Planet surface gravity log $g_{\rm p}$ (cgs)	3.69 ± 0.05
Orbital semi-major axis a (AU)	$0.534^{+0.012}_{-0.030}$
Orbital distance at periastron $a_{\rm per}$ (AU)	$0.266^{+0.013}_{-0.014}$
Orbital distance at apoastron $a_{\rm apo}$ (AU)	$0.797^{+0.032}_{-0.054}$
Equilibrium temperature at the average distance $T_{\rm eq}$ (K)^b	347 ± 12

Notes. $^{(a)}$In the planet reference frame. $^{(b)}$Black body equilibrium temperature assuming a null Bond albedo and uniform heat redistribution to the night side.

From our stellar parameters, the radius ratio $R_{\rm p}/R_*$, and the RV semi-amplitude, we find that KOI-3680b has a radius $R_{\rm p} = 0.99^{+0.06}_{-0.07}\,R_{\rm Jup}$, a mass $M_{\rm p} = 1.93^{+0.19}_{-0.21}\,M_{\rm Jup}$, and thus a density $\rho_{\rm p} = 2.46^{+0.42}_{-0.36}$ g cm^{-3}. As mentioned above, the planet revolves around its host star on a considerably eccentric orbit, $e = 0.496 \pm 0.031$ (see Fig. 3). The system age is unconstrained. Finally, the stellar and planetary parameters provided by the DR25 *Kepler* catalogue (Thompson et al. 2018) also agree with ours.

Table 4. Times of KOI-3680b mid-transits.

Time ($BJD_{TDB}-2\,450\,000$)	Uncertainty (days)
5512.93007	0.00037
5654.17088	0.00045
5795.41176	0.00039
5936.65315	0.00056
6077.8953	0.0014
6219.13963	0.00053
6360.37864	0.00049

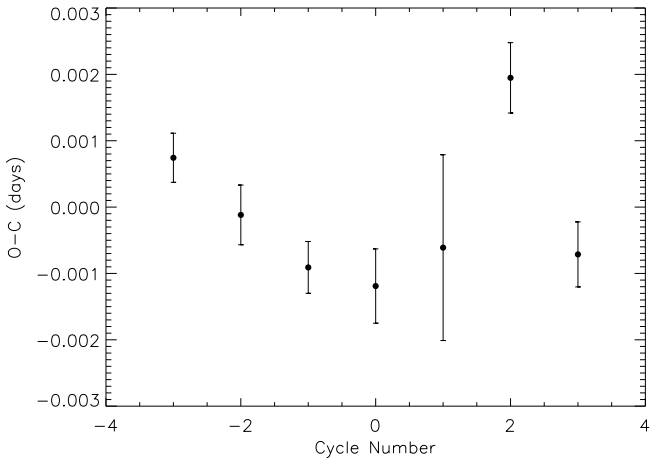

Fig. 6. Transit timing variations of KOI-3680b with respect to the linear ephemeris reported in Table 3.

3.3. Transit timing variations

The 141-day period is known with an uncertainty of only ±7.4 s. The tremendous accuracy offers an opportunity to search for any possible TTV. Such a TTV could be caused by additional companions and reveal a multiple planetary system.

In the same DE-MCMC Bayesian framework, we computed the individual transit times which are listed in Table 4. The transit epoch with the highest uncertainty refers to the fifth partial transit (Sect. 2.1). The derived TTVs and their error bars are shown in Fig. 6. They are similar to those determined independently by Holczer et al. (2016) and they present some marginal variations that would require more investigations and possible transit re-observations, which go beyond the scope of the present work. With the present data and analyses, we only detect and characterize the new planet KOI-3680b and could not report any significant detection of additional companions in the system.

As a sanity check, we performed an additional combined analysis as in Sect. 3.2 after correcting for the marginal mid-transit variations. This shown no significant differences in the resulting system parameters.

4. Discussion

Being a giant planet with a 5-month orbital period, KOI-3680b occupies a position in the parameters space where only a few planets are known today, in particular the transiting ones. The mass distribution in the total population of known exoplanets is bimodal with a gap around $M_p \sin i_p = 0.15\ M_{Jup}$. The distinction between those two populations of low-mass and giant planets is well known from RV surveys (e.g. Mayor et al. 2011). The mass valley has a corresponding radius valley seen in the population of transiting planets. These valleys are likely to be due to the ways giant planets grow depending on the mass of their core (e.g. Mordasini et al. 2012). It could be also partially due to evaporation processes and interactions with the host stars in the case of close-in planets (e.g. Owen & Wu 2017; Fulton et al. 2017; Van Eylen et al. 2018). The mass and radius of KOI-3680b put it in the giant planet population.

On the other hand, known giant planets show a bimodal distribution in their orbital periods, with close-in hot Jupiters at short periods and temperate giants at longer periods. The intermediate domain (periods between 10 and 100 days) shows a dearth of planets. That period valley was first identified by RV surveys (e.g. Udry et al. 2003) but was difficult to detect in the case of transiting planets (Santerne et al. 2016) as the latter method could be polluted by false positives and highly favours the detection of close-in planets. Indeed, only a few transiting, giant planets are known on orbital periods longer than a few tens of days. KOI-3680b is one of these rare cases.

Whereas several known transiting exoplanets have orbital periods longer than that of KOI-3680b (Rowe et al. 2014; Morton et al. 2016; Giles et al. 2018), only a few of them are well characterized, in particular with a mass measurement. Measured masses and orbital periods of transiting planets are plotted in Fig. 7[2], where giants are on the upper part. Plotted in red, KOI-3680b has parameters similar to five other giant planets: HD 80606b (P = 111.4 days), CoRoT-9b (P = 95.3 days), and KOI-1257b (P = 86.6 days) with masses also measured from radial velocities (Hébrard et al. 2011; Santerne et al. 2014; Bonomo et al. 2017a), and Kepler-30c (P = 60.3 days) and Kepler-87b (P = 114.7 days) with masses measured through TTVs (Fabrycky et al. 2012; Ofir et al. 2014). In that six-planet group, KOI-3680b has the longest period. Two giant planets with slightly lower mass have longer periods in Fig. 7: Kepler-16b (P = 228.8 days) and Kepler-34b (P = 288.8 days) which are circumbinary planets with TTV-measured masses (Doyle et al. 2011, Welsh et al. 2012). Therefore, to date, KOI-3680b is the known transiting giant planet with the longest period characterized around a single star.

Larger distances to the host stars imply lower planetary temperatures. In the case of KOI-3680b, the black-body equilibrium temperature at the average distance is T_{eq} = 347 ± 12 K (310 and 530 K at apastron and periastron, respectively), assuming a null Bond albedo and uniform heat redistribution to the night side (e.g. Alonso et al. 2009). Figure 8 shows equilibrium temperatures T_{eq} of known giant planets and their corresponding bulk densities. The plotted T_{eq} should be taken with caution as the actual T_{eq} values would depend on albedos and heat redistributions which vary from one planet to another, as well as on star–planet distances which vary for eccentric orbits. Nevertheless, the T_{eq} values plotted in Fig. 8 provide useful orders of magnitude and indicate that KOI-3680b is one of the rare temperate planets to be well characterized with measured mass and density. The distribution suggests a decreasing lower envelope which shows that the less-dense giant planets have higher temperatures. This trend should be taken with caution as there are only a few points below T_{eq} = 800 K. Still, Jupiter and Saturn are both located near that lower envelope. If real, this trend would agree with the tendency of hotter planets to have inflated radii (e.g. Fortney et al. 2007; Enoch et al. 2012).

[2] Figures 7 and 8 are based on the Exoplanet Orbit Database at `exoplanets.org` (Han et al. 2014).

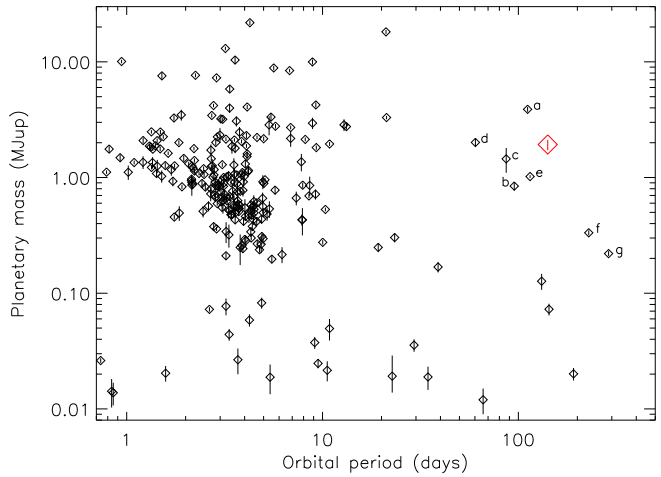

Fig. 7. Masses of transiting exoplanets as a function of their orbital periods. The figure only shows planets with radius and mass measured at better than ±30% each. The new planet KOI-3680b is plotted in red. Other planets discussed in the text are identified in the plot by letters *a* (HD 80606b), *b* (CoRoT-9b), *c* (KOI-1257b), *d* (Kepler-30c), *e* (Kepler-87b), *f* (Kepler-16b), and *g* (Kepler-34b).

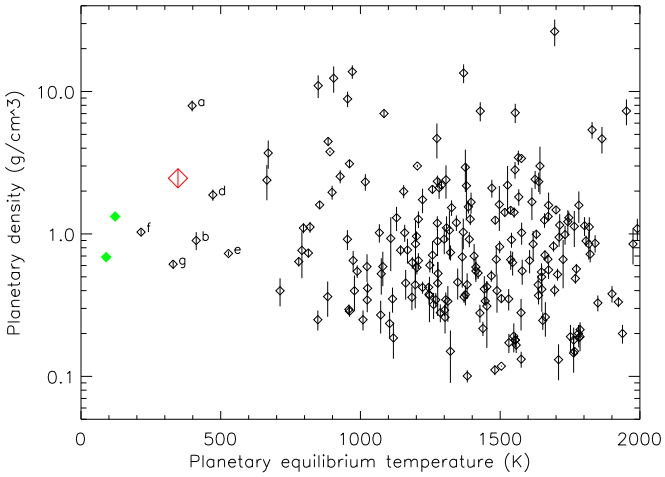

Fig. 8. Bulk density of giant planets as a function of their equilibrium temperature. Only known planets with a mass larger than 0.15 $M_{\rm Jup}$ and a density measured at better than ±50% are plotted here. The new planet KOI-3680b is plotted in red, and Saturn and Jupiter in filled green. Planets are labelled as in Fig. 7.

In Fig. 8, only two exoplanets have $T_{\rm eq}$ lower than that of KOI-3680b: they are the circumbinary planets Kepler-16b and Kepler-34b. Three others have slightly higher $T_{\rm eq}$ and lower densities: CoRoT-9b, Kepler-30c, and Kepler-87b. The planet HD 80606b has a slightly larger $T_{\rm eq}$ than that of KOI-3680b but a density three times greater. KOI-3680b is therefore among the colder giant planets characterized around a single star.

Figure 9 shows the position of KOI-3680b in the "modified" tidal diagram of transiting giant planets whose orbital eccentricities were uniformly determined by Bonomo et al. (2017b). In this diagram the $(P \times M_{\rm p}/M_{\rm s})$ quantity is plotted as a function of $(a/R_{\rm p})$; since the circularization timescales as $\tau_{\rm circ} \propto P \times M_{\rm p}/M_{\rm s} \times (a/R_{\rm p})^5$, eccentric orbits (blue squares for $e \geq 1$ in Fig. 9) are mostly expected at the right or upper-right part of the diagram, being almost unaffected by tidal dissipation/circularization. Indeed, they all lie beyond the 1-Gyr

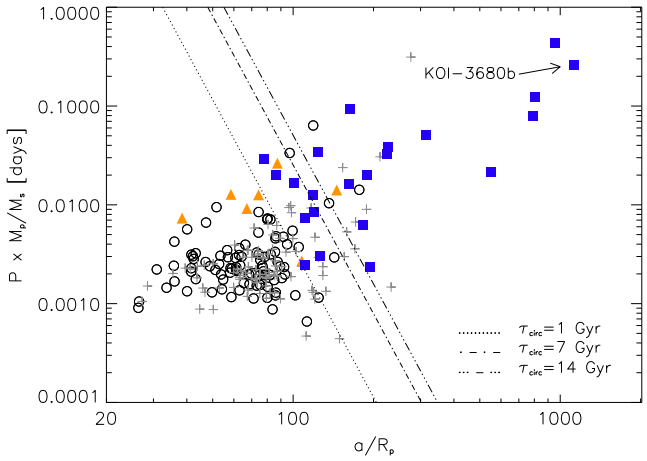

Fig. 9. "Modified" tidal diagram for 232 giant planets with uniformly derived eccentricities (Bonomo et al. 2017b). Black empty circles show the position of giant planets with well-determined circular orbits, i.e. with eccentricities consistent with zero and 1σ uncertainty $\sigma_e < 0.05$; grey crosses indicate planets with undetermined eccentricities which are usually consistent with zero but have large uncertainties $\sigma_e > 0.05$; orange triangles show small but significant eccentricities, i.e. $e < 0.1$; and blue squares $e \geq 0.1$. The position of KOI-3680b is indicated in the upper-right corner. The dotted, dash-dotted, and dash-three-dotted lines display the 1, 7, and 14 Gyr circularization timescales for a planetary modified tidal quality factor $Q'_{\rm p} = 10^6$ and $e = 0$, respectively.

circularization isochrone, and two-thirds of them beyond the 14-Gyr one (dash-three-dotted line in Fig. 9). KOI-3680b is currently the transiting giant planet with the largest $a/R_{\rm p}$ and mass measured through radial velocities, and is located at the upper-right corner of this diagram.

The high eccentricity of KOI-3680b does likely not originate from interactions with the protoplanetary disc, which tend to damp high eccentricities (e.g. Kley & Nelson 2012; Bitsch et al. 2013). Instead, it must be the outcome of evolution processes occurring after the disc dissipation, such as planet–planet gravitational scattering (e.g. Chatterjee et al. 2008), Kozai–Lidov perturbations caused by a distant stellar or planetary companion on a highly inclined orbit (e.g. Fabrycky & Tremaine 2007), and/or secular chaos in a multi-planet system (e.g. Wu & Lithwick 2011). Carrying on the RV follow-up of this system might unveil additional outer companions and clarify which is the most likely mechanism that gave rise to the high orbital eccentricity, as is the case for CoRoT-20b (Rey et al. 2018).

In terms of interior structure and evolution, KOI-3680b appears normal, that is, given the large uncertainty on its age, evolution models (Guillot 2005; Guillot et al. 2006) are able to match the observed radius both when assuming a solar composition and no core or a massive central core up to 140 $M_\oplus$. The contraction of the planet is still relatively significant (compared to hot Jupiters for which cooling is slowed by their irradiation): the planet contracted by about 0.06 $R_{\rm Jup}$ between the ages of 1 and 10 Gyr. This implies that a more precise determination of the stellar age (and generally of stellar parameters) would certainly yield useful constraints on the composition of this planet.

The new transiting planet KOI-3680b could allow characterizations in the mostly unexplored domain of temperate planets. Whereas most of the atmospheric studies are made in close-in planets, they could be feasible here in a more temperate domain, closer to that of Jupiter or Saturn. They would require extremely

large telescopes however, such as for example the Thirty Meter Telescope, due to the faintness of the host star. Still, due to the lower temperature, the scale height of the atmosphere is expected to be two to four times smaller than for close-in, giant planets, resulting in a shallower absorption signal. The emitted light detectable through occultations would also be smaller than that of hotter planets. In terms of obliquity measurement, the amplitude of the Rossiter–McLaughlin anomaly is expected to be on the order of 35 $m\,s^{-1}$. Such accuracy is barely reachable with SOPHIE due to the magnitude of the star, but this is feasible with a stable spectrograph mounted on a larger, more sensitive telescope such as HARPS-N at TNG or HIRES at Keck. The long duration of the transits (6.7 h) allows for more RV measurements to be obtained during a transit, but make it harder to find a transit fully observable during a given night. Combined observations of a given transit with different telescopes shifted in longitude or observations of different transits could help here (e.g. Hébrard et al. 2011).

Finally, with its long orbital period in comparison to most known transiting giant planets, KOI-3680b has a large Hill sphere of about 3.5 million kilometers, where the gravity of the planet dominates the gravity of the star. That extended sphere of gravitational influence makes the presence of satellites and rings around KOI-3680b more likely. Indeed, satellites must be included well within the Hill sphere to have stable orbits, and stable prograde orbits are typically within about 0.4 times the radius of the Hill sphere (e.g. Hinse et al. 2010). In addition, giant planets are more likely to host satellites and rings, as in the solar system. We note however that if the high eccentricity of KOI-3680b is due to dynamical instabilities, this may be detrimental for possible moons (e.g. Bonomo et al. 2017a; Lecavelier des Étangs 2017). Nevertheless, KOI-3680b is today one of the rare known systems favourable for the search of such structures, whereas most transiting planets have short periods and extremely tight Hill spheres of a few planetary radii. This probably explains the lack of satellites and rings detection outside the solar system. Today, the only known cases are the possible exomoon Kepler-1625b I (Teachey & Kipping 2018) and the suspected ring system in J1407 (Mamajek et al. 2012).

5. Conclusions

Following identification by the *Kepler* team as a promising candidate, we have established the planetary nature of the KOI-3680.01 transits and characterized this exoplanetary system. Its orbital period of 141 days, located between those of Mercury and Venus, makes KOI-3680b the known transiting, giant planet with the longest period characterized today around a single star. It offers opportunities to extend follow-up studies of exoplanets farther from their stars, and to compare close-in and more temperate planets. After the announcement of the present results, the *Kepler* Team gave the system KOI-3680 the name Kepler-1657 (Table 1).

With its 4-yr continuous observations, the *Kepler* mission was one of the rare experiments particularly favourable to the detection of long-period, transiting planets. Other programs including CoRoT, K2, Cheops, and ground-based surveys are less sensitive to such a range of periods due to the shorter durations of their continuous observations. Mainly PLATO (Rauer et al. 2014) and surveys secured from Antartica (e.g. Crouzet et al. 2018) could be able in the future to detect numerous transiting planets on longer periods. Whereas it monitors most of the sky with durations of 27 days only, the recently launched TESS satellite acquires photometry on longer time spans for a few parts of the sky, and therefore might also detect some long-period, transiting planets (e.g. Sullivan et al. 2015; Villanueva et al. 2018) which could eventually be characterized.

Acknowledgements. This publication is based on observations collected with the NASA *Kepler* mission and the SOPHIE spectrograph on the 1.93-m telescope at Observatoire de Haute-Provence (CNRS), France. We thank all the OHP staff of for their support. This work was supported by the "Programme National de Planétologie" (PNP) of CNRS/INSU, the Swiss National Science Foundation, the French National Research Agency (ANR-12-BS05-0012), FEDER – Fundo Europeu de Desenvolvimento Regional funds through the COMPETE 2020 – Programa Operacional Competitividade e Internacionalização (POCI), and by the Portuguese funds through FCT – Fundação para a Ciência e a Tecnologia in the framework of the projects POCI-01-0145-FEDER-028953 and POCI-01-0145-FEDER-032113. N.C.S. further acknowledges the support from FCT through national funds and by FEDER through COMPETE2020 by these grants UID/FIS/04434/2013 and POCI-01-0145-FEDER-007672. A.S.B. acknowledges funding from the European Union Seventh Framework Programme (FP7/2007-2013) under Grant Agreement No. 313014 (ETAEARTH). S.C.C.B. acknowledges support from FCT through Investigador FCT contract IF/01312/2014/CP1215/CT0004.

References

Almenara, J. M., Damiani, C., Bouchy, F., et al. 2015, A&A, 575, A71
Almenara, J. M., Díaz, R. F., Hébrard, G., et al. 2018, A&A, 615, A90
Alonso, R., Alapini, A., Aigrain, S., et al. 2009, A&A, 506, 353
Baranne, A., Queloz, D., Mayor, M., et al. 1994, A&AS, 119, 373
Batalha, N. M., Rowe, J. F., Bryson, S. T., et al. 2013, ApJS, 204, 24
Beatty, T. G., & Gaudi, B. S. 2008, ApJ, 686, 1302
Berger, T. A., Huber, D., Gaidos, E., & van Saders, J. L. 2018, ApJ, 866, 99
Bitsch, B., Crida, A., Libert, A.-S., & Lega, E. 2013, A&A, 555, A124
Boisse, I., Eggenberger, A., Santos, N. C., et al. 2010, A&A, 523, A88
Bonomo, A. S., Santerne, A., Alonso, R., et al. 2010, A&A, 520, A65
Bonomo, A. S., Hébrard, G., Santerne, A., et al. 2012a, A&A, 538, A96
Bonomo, A. S., Chabaud, P.-Y., Deleuil, M. et al. 2012b, A&A, 547, A110
Bonomo, A. S., Sozzetti, A., Lovis, C., et al. 2014, A&A, 572, A2
Bonomo, A. S., Sozzetti, A., Santerne, A., et al. 2015, A&A, 575, A85
Bonomo, A. S., Hébrard, G., Raymond, S. N., et al. 2017a, A&A, 603, A43
Bonomo, A. S., Desidera, S., Benatti, S., et al. 2017b, A&A, 602, A107
Borucki, W. J., Koch, D. G., Basri, G., et al. 2011a, ApJ, 728, 117
Borucki, W. J., Koch, D. G., Basri, G., et al. 2011b, ApJ, 736, 19
Bouchy, F., Hébrard, G., Udry, S., et al. 2009a, A&A, 505, 853
Bouchy, F., Isambert, J., Lovis, C., et al. 2009b, EAS Pub Ser., 37, 247
Bouchy, F., Bonomo, A. S., Santerne, A., et al. 2011, A&A, 533, A83
Bouchy, F., Díaz, R. F., Hébrard, G., et al. 2013, A&A, 549, A49
Bruno, G., Almenara, J.-M., Barros, S. C. C., et al. 2015, A&A, 573, A124
Buchhave, L. A., Dressing, C. D., Dumusque, X., et al. 2016, AJ, 152, 160
Chatterjee, S., Ford, E. B., Matsumura, S., & Rasio, F. A. 2008, ApJ, 686, 580
Ciceri, S., Lillo-Box, J., Southworth, J., et al. 2015, A&A, 573, L5
Claret, A. 2004, A&A, 428, 1001
Crouzet, N., Chapellier, N., Guillot, T., et al. 2018, A&A, 619, A116
Czesla, S., Huber, K. F., Wolter, U., et al. 2009, A&A, 505, 1277
Deeg, H. J., Moutou, C., Erikson, A., et al. 2010, Nature, 464, 384
Deleuil, M., Almenara, J.-M., Santerne, A., et al. 2014, A&A, 564, A56
Demarque, W., & Kim, Y. 2004, ApJS, 155, 667
Díaz, R. F., Damiani, C., Deleuil, M., et al. 2013, A&A, 551, L9
Díaz, R. F., Montagnier, G., Leconte, J., et al. 2014, A&A, 572, A109
Dotter A., Chaboyer B., Jevremović D., et al. 2008, ApJS, 178, 89
Doyle, L. R., Carter, J. A., Fabrycky, D. C., et al., 2011, Science, 333, 1602
Eastman, J., Gaudi, B. S., & Agol, E. 2013, PASP, 125, 923
Ehrenreich, D., Lagrange, A.-M., Bouchy, F., et al. 2011, A&A, 525, A85
Enoch, B., Collier Cameron, A., & Horne, K, 2012, A&A, 540, A99
Fabrycky, D., & Tremaine, S. 2007, ApJ, 669, 1298
Fabrycky, F. C., Ford, E. B., Steffen, J. H., et al. 2012, ApJ, 750, 114
Ford, E. B., Ragozzine, D., Rowe, J. F., et al. 2012, ApJ, 756, 185
Fortney, J. J., Marley, M. S., & Barnes, J. W. 2007, ApJ, 659, 1661
Fulton, B. J., Petigura, E. A., Howard, A. W., et al. 2017, AJ, 154, 109
Gaia Collaboration (Brown, A. G. A., et al.) 2018, A&A, 616, A1
Giles, H. A. C., Osborn, H. P., Blanco-Cuaresma, S., et al. 2018, A&A, 615, L13
Gregory, P. C. 2005, ApJ, 631, 1198
Guillot, T. 2005, Annu. Rev. Earth Planet Sci., 33, 493
Guillot, T., Santos, N. C., Pont, F., et al. 2006, A&A, 453, L21
Han, E., Wang, S. X., Wright, Jason T., et al. 2014, PASP, 126, 827
Hébrard, G., Bouchy, F., Pont, F., et al. 2008, A&A, 481, 52
Hébrard, G., Désert, J.-M., Díaz, R. F., et al. 2011, A&A, 516, A95

Hébrard, G., Santerne, A., Montagnier, G., et al. 2014, A&A, 572, A93
Hinse, T. C., Christou, A. A., Alvarellos, J. L. A., & Goździewski, K. 2010, MNRAS, 404, 837
Holczer, T., Mazeh, T., Nachmani, G., et al. 2016, ApJS, 225, 9
Holman, M. J., Fabrycky, D. C., Ragozzine, D., et al. 2010, Science, 330, 51
Jenkins, J. M., Caldwell, D. A., Chandrasekaran, H., et al. 2010, ApJ, 713, L87
Kipping, D. 2010, MNRAS, 408, 1758
Kipping, D. 2013, MNRAS, 435, 2152
Kley, W., & Nelson, R. P. 2012, ARA&A, 50, 211
Kurucz, R. 1993, SYNTHE Spectrum Synthesis Programs and Line Data (Cambridge, MA: Smithsonian Astrophysical Observatory), 13
Lecavelier des Étangs, A., Hébrard, G., Blandin, S., et al. 2017, A&A, 603, A115
Lissauer, J. J., Marcy, G. W., Rowe, J. F., et al. 2012, ApJ, 750, 112
Lissauer, J. J., Marcy, G. W., Bryson, S. T., et al. 2014, ApJ, 784, 44
Mamajek, E. E., Quillen, A. C., Pecaut, M. J., et al. 2012, AJ, 143, 72
Mandel, K., & Agol, E. 2002, ApJ, 580, L171
Marcy, G. W., Isaacson, H., Howard, A. W., et al. 2014, ApJS, 210, 20
Mordasini, C., Alibert, Y., Georgy, C., et al. 2012, A&A, 547, A112
Morton, T. D., Bryson, S. T., Coughlin, J. L., et al. 2016, ApJ, 822, 86
Moutou, C., Hébrard, G., Bouchy, F. , et al. 2009, A&A, 498, L5
Moutou, C., Bonomo, A. S., Bruno, G., et al. 2013, A&A, 558, L6
Mayor, M., Marmier, M., Lovis, C., et al., 2011, ArXiv e-prints [arXiv:1109.2497]
Ofir, A., Dreizler, S., Zechmeister, M., & Husser, T.-O. 2014, A&A, 561, A103
Owen, J. E., & Wu, Y. 2017, ApJ, 847, 29
Pepe, F., Mayor, M., Galland, F., et al. 2002, A&A, 388, 632
Perruchot, S., Kohler, D., Bouchy, F., et al., 2008, Proc. SPIE, 7014, 70140
Rauer, H., Catala, C., Aerts, C., et al. 2014, Exp. Astron., 38, 249
Rey, J., Bouchy, F., Stalport, M., et al. 2018, A&A, 619, A115
Rowe, J. F., Bryson, S. T., Marcy, G. W., et al. 2014, ApJ, 784, 45
Rowe, J. F., Coughlin, J. L., Antoci, V., et al. 2015, ApJS, 217, 16
Sanchis-Ojeda, R., Fabrycky, D. C., Winn, J. N., et al. 2012, Nature, 487, 449
Santerne, A., Díaz, R. F., Bouchy, F., et al. 2011, A&A, 528, A63
Santerne, A., Díaz, R. F., Moutou, C., et al. 2012, A&A, 545, A76
Santerne, A., Hébrard, G., Deleuil, M., et al. 2014, A&A, 571, A37
Santerne, A., Moutou, C.. Tsantaki, M., et al. 2016, A&A, 587, A64
Santos, N. C., Sousa, S. G., Mortier, A., et al. 2013, A&A, 556, A150
Sneden, C. 1973, Ph.D. Thesis (Austin: University of Texas)
Sousa, S. G., Santos, N. C., Mayor, M. et al. 2008, A&A, 487, 373
Sullivan, P. W., Winn, J. N., Berta-Thompson, Z. K., et al. 2015, ApJ, 809, 77
Ter Braak C. J. F. 2006, Stat. Comput., 16, 239
Teachey, A., & Kipping, D. M. 2018, Sci. Adv., 4, eaav1784
Thompson, S. E., Coughlin, J. L., Hoffman, K., et al. 2018, ApJS, 235, 38
Torres, G., Andersen, J., & Giménez, A. 2010, A&ARv, 18, 67
Udry, S., Mayor, M., & Santos, N. C. 2003, A&A, 407, 369
Van Eylen, V., Agentoft, C., Lundkvist, M. S., et al. 2018, MNRAS, 479, 4786
Villanueva, S Jr., Dragomir, D., & Gaudi, B. S. 2018, ArXiv e-prints [arXiv:1805.00956]
Wang, J., Fischer, D. A., Barclay, T., et al. 2013, ApJ, 776, 10
Welsh, W. F., Orosz, J. A., Carter, J. A., et al. 2012, Nature, 481, 475
Winn, J. N. 2010, exop.book, 55 [arXiv:1001.2010]
Wu, Y., & Lithwick, Y. 2011, ApJ, 735, 109
Zechmeister, M., & Kürster, M. 2009, A&A, 496, 577